

Topic
Decision Aids/Supports and Data Fusion

Title
**Coastal Activity Monitoring with Evidential Fusion of Contextual Attributes
from Multi-Pass RadarSAT-1 Data**

Alexandre JOUAN
Lockheed Martin Canada
6111 Royalmount Avenue, Montreal QC H4P 1K6
Tel : (514) 340 8310 #8442
Email : alexandre.jouan@lmco.com

Yannick ALLARD
Lockheed Martin Canada
6111 Royalmount Avenue, Montreal QC H4P 1K6
Tel : (514) 340 8310 #7776
Email : yannick.allard@lmco.com

Yves MARCOZ
Centre de Recherches Mathematiques
Universite de Montreal

Point of contact: Alexandre JOUAN

Coastal Activity Monitoring using Evidential Fusion of Contextual Attributes from Multi-Pass RADARSAT-1 Data¹

Alexandre Jouan (1), Yannick Allard (2), Yves Marcoz (3)

(1-2) Lockheed Martin Canada

6111 Royalmount Avenue, Montreal (QC) H4P 1K6

(514) 340-8310 ext. 8442 (1), 7772 (2)

alexandre.jouan@lmco.com; yannick.allard@lmco.com;

(3) Centre de Recherches Mathematiques

Universite de Montreal

yves@marcoz.org

Abstract

As part of the second edition of the Application Development and Research Opportunity (ADRO2) program sponsored by the Canada Space Agency, Lockheed Martin Canada has developed a system for coastal activity monitoring using evidential fusion of contextual attributes. These attributes are provided by texture classifiers, change detectors or GIS themes. This system has the capability of detecting and classifying changes in order to locate and highlight regions of potential concerns.

The proposed system processes a set of multi-date RADARSAT-1 acquisitions with change detectors and textural classifiers. Classifiers are used to build hypotheses on a set of contextual attributes that are combined using evidence theory. This combination strategy is the core of the fusion process. It provides a powerful information management tool for the fusion of imprecise, incomplete and inaccurate data. The role of the fusion system is to provide the most accurate representation of the knowledge gathered on the scene to assist the operator in taking a decision.

This paper present the results obtained on seven scenes acquired over Stephenville, NF (48°31N, 58°32W), processed as SSG maps in UTM projection. GIS data sets were ordered from the National Topographic Data Base and extracted using GRASS software. Coregistration of the temporal data has been performed by correlating several sub-regions of the scenes with Fourier Transform.

1. Introduction

Lockheed Martin Canada has developed over the years various applications in multi-sensor data fusion. Initially focused on developing a data fusion test-bed for the Canadian Patrol Frigate integrating elements of the JDL fusion levels 0-4, this activity has been extended to the simulation of typical Mission Management Systems for surveillance aircraft. For this purpose, a data fusion simulation test-bed was built demonstrating the fusion of target related features obtained by processing Synthetic Aperture Radar (SAR) imagery and other source of information provided by non imaging sensors.

¹ This work is sponsored by the Canadian Space Agency under the Applications Development and Research Opportunities Program (ADRO-2) project #20, and Lockheed Martin Canada

These test-beds have in common the same objective: studying under which conditions a data fusion system could provide as complete a description of the scene as possible, the most precise identification of the surrounding targets while being robust to confusion.

These projects were helpful to demonstrate how the performance of target detection/target recognition (TR/TD) algorithms could be significantly improved by incorporating contextual information.

Several studies have already shown that RADARSAT-1 would provide valuable information for coastal surveillance missions and activity monitoring. Based on the expertise gained on the data fusion projects, we proposed to develop a methodology for change monitoring based on the fusion of contextual features extracted from multi-pass imagery. The following sections describe the main aspects and results obtained by the proposed approach.

As part of the second edition of the Application Development and Research Opportunity program (ADRO2) sponsored by the Canadian Space Agency, Lockheed Martin Canada has proposed to develop a system for coastal activity monitoring based on the evidential fusion of contextual attributes extracted from multi-pass RADARSAT-1 imagery.

The proposed system contains classifiers that are used to build hypotheses on a generic set of contextual attributes (water, wetland, shore, vegetation, fields, man-made objects,...). The hypotheses are further combined using evidence theory. This combination strategy is the core of the fusion process. It provides a powerful information management tool for the combination of imprecise, incomplete and inaccurate data.

Section 2 describes a preprocessing step needed to make use of incomplete GIS databases as a priori information.

Section 3 describes the data fusion system designed for land-use mapping and activity monitoring using evidential fusion.

Section 4 shows the results obtained on the data set provided by the Canadian Space Agency as part of the Application Development and Research Opportunity (ADRO) program.

Section 5 concludes the work and presents the highlights of a current project that enlarge the proposed data fusion system to multi sensor applications.

2. A priori Information

The study site is located around the airport of Stephenville, Newfoundland.

Table 1 provides information about the acquisitions provided by the Canadian Space Agency through the Application Development and Research Opportunity (ADRO) program.

Scene #	Dataset	Date	Beam	Orbit	Proj.	Corr.	Pixel/Line Spac.(m)
Scn2	C0016820	1997/11/20	F2F	Asc	UTM-WGS84	SSG	6.25/6.25
Scn3	C0016809	1998/05/14	F2	Asc	UTM-WGS84	SSG	6.25/6.25
Scn4	C0016811	1998/05/21	F1	Asc	UTM-WGS84	SSG	6.25/6.25
Scn1	C0016960	1998/06/14	F1	Asc	UTM-WGS84	SSG	6.25/6.25
Scn5	C0017335	2000/08/31	F2	Asc	UTM-WGS84	SSG	6.25/6.25
Scn6	C0017338	2000/09/01	F4	Desc	UTM-NAD83	SSG	6.25/6.25
Scn7	C0019852	2001/04/28	F2	Asc	UTM-WGS84	SSG	6.25/6.25

Table 1. RADARSAT-1 Acquisitions.

In addition to remotely sensed imagery, themes from Geographical Information System (G.I.S) or weather information provided by Environment Canada can be useful sources of information to improve the interpretation of the backscattered signal from the ground.

Table 2 provides environmental conditions at the time acquisitions provided by Environment Canada and the Canadian Hydrographic Service.

However, data provided in G.I.S files may not necessarily correspond to the situation on the ground. It may be inaccurate, outdated or in case of natural disaster (such as floods) difficult to use without an appropriate processing. For this reason, a preprocessing step has been designed in order to make a more efficient use of incomplete GIS files.

Scene #	Dataset	Date	Tide (m)	Wind (km/h)	RH (%)	Temp (C)	Total Daily Rainfall	Total Daily Snowfall	Snow on Ground (cm)
Scn2	C0016820	1997/11/20	-	9	70	0.1	0	0	3
Scn3	C0016809	1998/05/14	0.982	4	53	10.0	0	0	0
Scn4	C0016811	1998/05/21	0.881	7	69	13.7	0	0	0
Scn1	C0016960	1998/06/14	0.607	9	80	11.7	0	0	0
Scn5	C0017335	2000/08/31	1.001	13	87	17.1	0	0	0
Scn6	C0017338	2000/09/01	1.0	-	-	-	-	-	-
Scn7	C0019852	2001/04/28	0.471	9	82	-1.2	34.8	1.2	0

Table 2. Environmental conditions provided by the Atlantic Climate Center of Environment Canada and the Canadian Hydrographic Services (Bedford Institute of Oceanography) for Port Harmon.

2.1 Updating G.I.S Files

We used a Markov random field model to fuse the information derived from RADARSAT-1 imagery and ancillary data from a G.I.S. database. Since the ground cover map of the studied region is incomplete, the regions without information have been labeled using a stochastic labeling and a relaxation of the decision with an Iterated Conditional Mode (ICM) approach. The output is then used to initiate a classification procedure in a multi-temporal context to derive a time varying land-use mapping for land-use monitoring.

The information used in the classification process consists in : 1) a partially complete ground cover map provided by the G.I.S. database; 2) a set of textural parameters derived from the Grey Level Co-occurrence Matrix (GLCM); 3) the radiometric intensity.

In the first step of the process, the “no data” region of the G.I.S. ground cover map has been labeled using the first available radar image without allowing the existing cluster to change. A stochastic labeling operation has been performed using a pseudo-random initialization of those regions. By pseudo-random, we mean that the random initialization of the class labels has been constrained for some classes (here the airport, where random airport labels are only allowed to take place in a close distance of it, the distance map being computed from the G.I.S. data).

The image data model used here is very simple since it is based on the gray level of the image and can therefore be applied to any kind of images. We applied the MAP estimator of the label space, which maximize the *a posteriori* probability:

$$P(\mathbf{w}|F) = \frac{1}{P(F)} P(F|\mathbf{w}) P(\mathbf{w})$$

where F is the observed image, \mathbf{w} is the set of all possible labels and where $P(F)$ only depends on the observations and where we suppose that :

$$P(F|\mathbf{w}) = \prod_{s \in S} P(f_s | \mathbf{w}_s)$$

where f_s is the observed pixel at site s and \mathbf{w}_s it's label. We will use the equivalence between Markov random fields and Gibbs distributions to work with local potential energy instead of the global energy of the system. The *a priori* probability will therefore be written in the form of :

$$P(\cdot) = \frac{1}{Z} \exp -U(\cdot)$$

where U is the energy function and Z is a normalization constant.

The energy function to minimize is :

$$U = \sum_{a=1}^A U_{data(a)} + U_{spatial, map}$$

where :

$$U_{data} = \sum_{s \in S} \left(\ln(\sqrt{2\pi} \mathbf{s}_{\mathbf{w}_s}) + \frac{(f_s - \mathbf{m}_{\mathbf{w}_s})^2}{2\mathbf{s}_{\mathbf{w}_s}^2} \right)$$

and

$$U_{spatial, map} = U_{spatial} + U_{map}$$

where

$$U_{spatial} = - \sum_{\{s,r\} \in C} \mathbf{b}d(\mathbf{w}_s, \mathbf{w}_r)$$

where the parameter \mathbf{b} controls the homogeneity of the regions.

On the other hand, U_{map} correspond to the map transition model, which controls the transition from one class to another using a priori knowledge to define the Class Conditional Transition Probabilities (CCTP) and is given by

$$U_{map} = -\mathbf{b}_{map} \sum_{\{s,r\} \in C} t(\mathbf{w}_s | \mathbf{w}_r)$$

where $t(\mathbf{w}_s | \mathbf{w}_r)$ is the probability of transition from class \mathbf{w}_s to class \mathbf{w}_r between the time of creation of the map and the current time.

2.1.1 Choice of the Neighborhood Topology and Optimization Algorithm

Two different neighborhood configurations were tested, namely the classical 8-connectivity and the 8-connectivity "with holes" as shown on Figure 1.

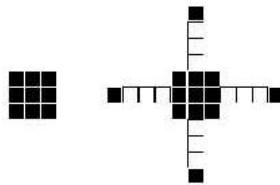


Figure 1: Classical and with holes topology

Four different stochastic optimization algorithms were tested for the energy minimization task:

- the Metropolis algorithm [Kirkpatrick, 1983],
- the Gibbs sampler [Geman, 1984],
- the Modified Metropolis Dynamics (MMD) [Kato, 1997],
- the Polya urn sampling model (super urn case) [Banerjee and al., 1999].

The hyperparameter, which controls the homogeneity of the segmentation, has been fixed to 0.45 in the classical topology and 0.3 in the topology with holes to account for the increase in the number of considered neighbors. Table 2 shows the results of a simulation conducted on the test image shown Figure 2 (ground truth is shown Figure 3).

	Classical		With Holes	
	time/iteration	%	time/iteration	%
Metropolis	1.89	92.9	1.93	96.5
MMD	1.35	92.8	1.39	96
Gibbs	2.71	97.1	2.78	97.5
Polya	5.9	59.6	6.9	60.1

Table 2. Optimization results

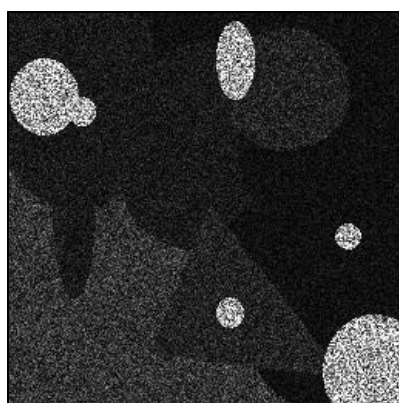


Figure 2. Test image



Figure 3. Class labels

Table 2 clearly shows that the neighborhood topology with holes performs better than the classical one. As stated by Pony [Pony & al., 2000], this topology destroys stable but undesirable small structures. Despite a little increase in the computing time, we will use the topology with holes for the rest of this work.

With respect to the optimization algorithm, we observed that the Polya urn sampling scheme is unsuitable for the task in a very noisy environment since it naturally emphasizes the majority labels in a given neighborhood. The computation time required for the Gibbs sampler is about twice that of the other tested Simulated Annealing-type algorithms and is therefore unsuitable in an operational context. The MMD algorithm will be used for the rest of the study since it provides the best compromise between precision of the resulting segmentation and required computation time.

The deterministic temporal relaxation labeling will be performed with the ICM algorithm [Besag, 1986]. This algorithm is relatively fast and should perform quite well since the resulting segmentation of the MMD is expected to be of good quality.

2.1.2 Results on RADARSAT-1 Imagery

Figure 4 shows the selected study site (City of Stephenville and vicinity, Newfoundland).

Figure 5 shows the color coding of the six selected land-use classes: airport, water, wetland, vegetation, grass and town.

Figure 6 shows the available cover map with the data as extracted from the G.I.S files provided by Geomatics Canada. Note that the black area corresponds to regions for which G.I.S files do not provide any information.

Figure 7 shows the result of the pseudo-random initialization.

Figure 8 shows the result of the stochastic labeling of the "no G.I.S. data" region, i.e. the black area in Figure 6. Stochastic labeling has been used for the initialization of the ICM algorithm for the temporal relaxation labeling. The result of this operation is shown Figure 9.

After that, all subsequent results of the ICM at time T is used for the initialization on the image taken at time T+1. This technique will provide a land-use map for each image available that can be used for change detection (change detection by post-classification comparison).

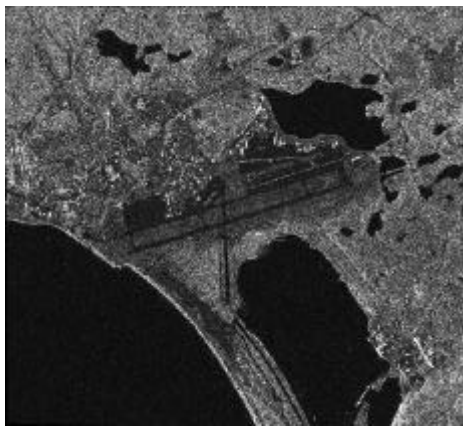


Figure 4. Original image



Figure 5. Classification labels

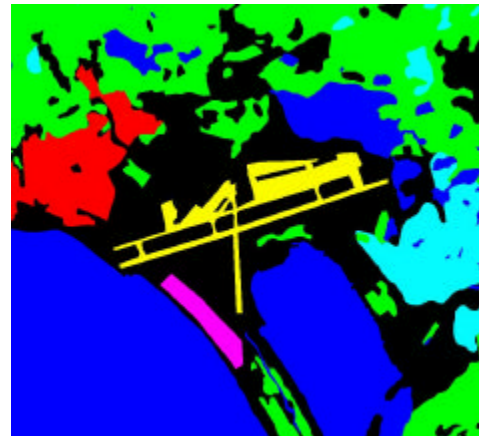


Figure 6. Incomplete land-use map

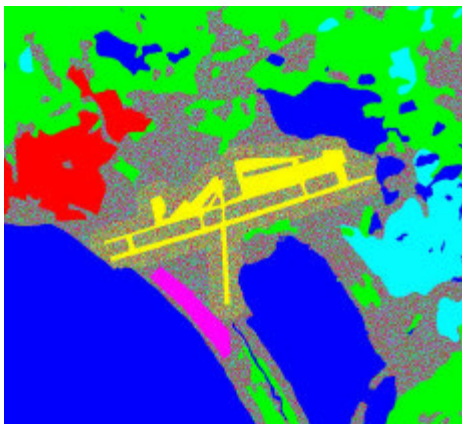


Figure 7. Pseudo-random initialization

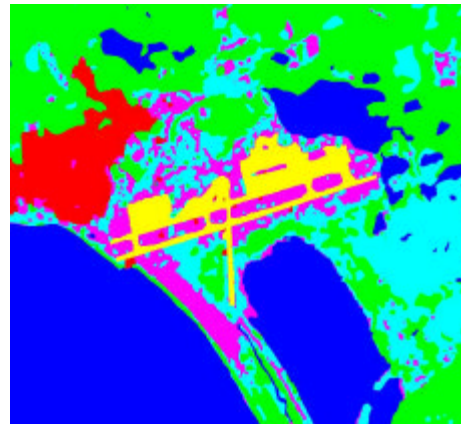


Figure 8. Stochastic labeling of the "no G.I.S. data" regions

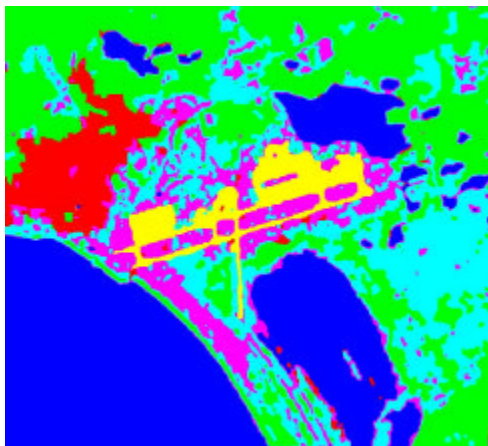


Figure 9. Result of the first deterministic relaxation (without CCTP)

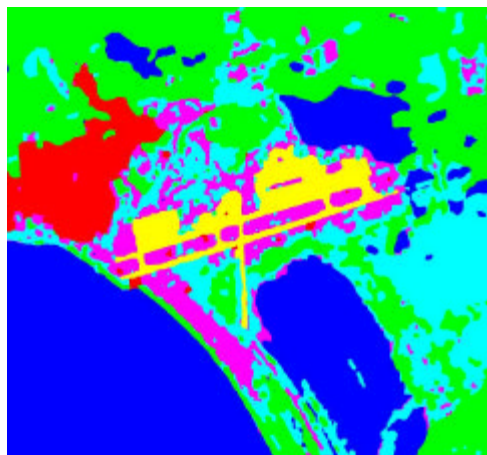


Figure 10. Deterministic relaxation T1 (with CCTP)

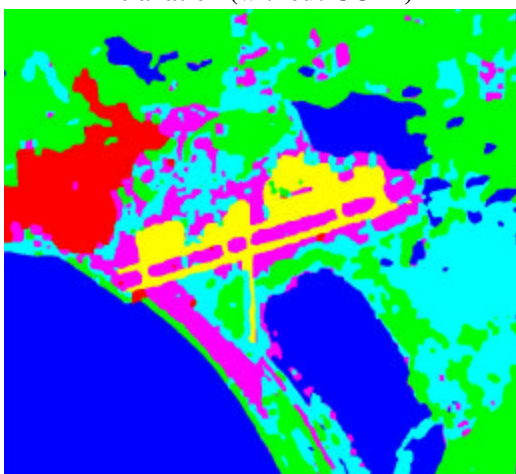


Figure 11. Deterministic relaxation T2 (with CCTP)

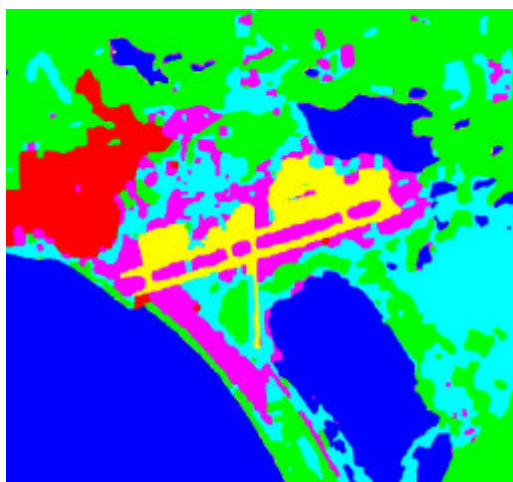


Figure 12. Deterministic relaxation T3 (with CCTP)

Following those results, we can see that buildings (characterized by strong scatterers) are misclassified as vegetation. This is due to an inaccurate estimation of the parameters of this class obtained from the GIS layer of built-up area. This layer also includes grass, trees, buildings as well as roads and a lot of dark structures. The estimated mean of the class building is lower than it should be and the variance is greater. The estimated parameters of the class buildings are then much closer to those of the class vegetation. Several options exist to avoid such a misclassification. As an example, a sub-class of the G.I.S layer "building" called "man-made structure" could be defined that would provide a more accurate estimation of the corresponding parameters. Another approach would be to fuse the result of a specular reflector detector with the previous result to obtain a more consistent interpretation.

3. Land Use Mapping and Activity Monitoring using Evidential Fusion

Textural analysis is performed with a neural network (multi-layer perceptron) trained to classify pixels into contextual classes from a set of eight textural features computed from the Gray Level

Co-Occurrence Matrix. The number of textural features used as input to the neural network is optimized using genetic algorithms.

The output of neural network is a pixel-based distribution of weights associated to each contextual class. This output can be used to generate a map by giving each pixel the label associated to the larger weight. However, the pixel-based distribution of weights must be kept in memory for further combination with the output of the textural classifier executed on another acquisition. This combination is performed with evidential fusion using Dempster-Shafer theory. Rule-based reasoning is also used to interpret class variations and discriminate between the changes due to acquisition parameters (the same object seen differently due to different acquisition conditions) or those due to the apparition of new structures.

As an example, with only two images from the data set, two bridges were crossing a river but only one of them was clearly identified on one of the two acquisitions. However, these two bridges were successfully detected on the second acquisition taken at a later date but with a slightly different incidence angle. Rules were implemented to interpret the class switching as the result of different acquisition parameters rather than the detection of an unknown object. Natural changes are also processed through rule-based reasoning sometimes leading to the creation of a new class (i.e. a class called “sand” which typically corresponds to area that are temporarily submerged). Figure 15 shows that the detection of a man made object on an area known as the TransCanada Highway led to the detection of a potential vehicle.

3.1 Hierarchical Classifier

The selected classifier is a multi-layer perceptron with eight neurons on the input layer, fourteen neurons on the hidden layer and four neurons on the output layer.

The neural network is trained using a base of training vectors selected to be as representative as possible of all the classes. This step is critical to have good performance, because of the high dependency of the classifier on the training base. We selected our training database from the scene 2 (Table 1), from the Stephenville Crossing area, labeling the vectors according to various GIS themes. Even with the help of GIS themes, a visual selection of the vectors is necessary, to make sure that no pixel is labeled in the wrong class. For example, on a zone mapped as ocean by the GIS, there might be ships at the time of acquisition that shouldn't be included in the training vectors, or else the performance would significantly decrease. The output of the classifier consists in four values ranged from 0 to 1. Each value corresponds to a confidence level that the current pixel belongs to the classes (1 meaning it belongs to this class, and 0 meaning it does not).

The first set of contextual features is the textural features computed from the Grey Level Co-occurrence Matrices (GLCM). The number of gray level for each SAR image was reduced to 11 and the matrices were computed using a 9x9 pixel neighborhood window.

For each GLCM, a set of height parameters is computed and used as the input of a neural network trained to classify textures in four different classes namely water, wetland/short grass, vegetation, man-made objects. The output of the network is a set of four values representing the confidence that the studied pixel belongs to the associated class.

From the output of the classifier, two types of analysis can be made.

First, a *thematic map* can be built by labeling pixels according to the highest output of the classifier. Figure 1 shows a typical result of such thematic mapping.

Another approach is to build a *pixel-based declaration* (in the Dempster-Shafer sense) from the whole set of confidence values. Temporal monitoring can thus be performed through the fusion of such independent declarations obtained by the classifier on scenes taken at different time. In order to increase or decrease the level of confidence associated to the classification as well as to improve the interpretation of changes over time, the temporal declarations by using the Dempster-Shafer evidential reasoning.

3.1.1 Selection of GLCM Features using Genetic Algorithm

The set of eight textural features that have been selected for the classification are [Solberg, 1997] the maximum (MAX), the first-order difference moment (FDM), the second-order difference moment or inertia (SDM), the first-order inverse difference moment (FIDM), the second-order inverse difference moment (SIDM), the entropy (ENT), the uniformity or angular second moment (UNI) and the cluster shade (CLSH).

The selection of features has tested on 8 GLCM and 11 Gaussian Markov Random Field (GMRF) features [Chellappa and Chatterjee, 1984] using a simple genetic algorithm. Applied on airborne SAR imagery, these tests show that the GLCM features are performing better than the GMRF features, and that even though some features are not necessary, they do not decrease the performance either. These results need to be confirmed for space-borne imagery.

3.1.1.1 Fitness value

The fitness value is a measure of the performance of a chromosome. The goal here is to improve the texture classification for a test image. The resulting image of the classification is computed using the features selected by each chromosome. The classifier is a multi layer perceptron with 18 neurons on the hidden layer trained using selected regions for each zone in the test image. The percentage of good classification has been evaluated using the GIS data as ground truth. A linear transformation of this percentage is used as the fitness value for the chromosome. The main disadvantage of this type of classifier is the randomness of the initialization. Two training with the same training base will not necessarily give the same percentage of error (about 0.5% difference maximum) so it is difficult to compare two sets of features having close fitness values. This is generally not a big problem but can sometimes prevent the algorithm from converging properly to the optimal value.

3.1.1.2 Genetic operations

A population of twenty chromosomes is randomly generated at the beginning and several genetic operations are applied to them until a selected number of generation is reached.

The genetic operations are the crossover, the mutation and the reproduction.

The crossover operation consists in selecting pairs in the population, and to mix the genes of the chromosomes of a pair. We decided to choose the two points crossover for our application. This crossover consists in slicing each parent chromosome at 2 random points, and to replace the middle part of one chromosome by the middle part of the second chromosome. The crossover rate used is 90%.

The mutation operation is an inversion of a gene. Each gene has a probability of 1/50 to be mutated.

The reproduction step uses the biased roulette wheel. Each chromosome has its fitness value computed, and is given a probability of being selected proportional to its fitness value ($p_i = f_i / \sum_i f_i$ where f_i is the fitness value of the i^{th} chromosome).

Twenty new chromosomes are then selected among the offspring of the previous population.

3.1.1.3 Results

The algorithm has been stopped after 1000 generations. As expected, the algorithm did not converge to a single set of features but to several sets that are approximately equivalent. We thus took the 20 best chromosomes the algorithm found during the execution, and we selected what were the features (and the patterns of features) which were the most frequent among those chromosomes. Table 3 presents the 20 best chromosomes computed, with the associated error percentage. We are now able to determine what features played a significant role for the classification, and what features is useless, or even disturbing the classifier. So, we can see that among the GLCM features, 5 are much more significant than the others that are the SDM, SIDM, ENT, UNI and CLSH. This confirms the results obtained by [Solberg, 1997] where SDM, SIDM and CLSH were among the best features for satellite SAR images. For the GMRF features, the 1st, 3rd, 4th, 5th, 8th, 9th and 11th features are significant compared to the others.

Error percentage	GMRF features	GLCM features
12.78	10010001101	00101111
12.77	10110011101	00111111
12.76	11110011100	10101101
12.76	10111011001	00101101
12.74	10110011001	10111111
12.73	10011011001	00111111
12.72	10110011011	00111111
12.70	10111001011	10101111
12.67	10011001101	00101111
12.65	00111001011	00101111
12.65	10110011001	00101111
12.64	10111011001	00101111
12.63	00111011011	00101111
12.59	11110011010	01101111
12.58	10110011101	00101111
12.56	00111011000	10101111
12.56	10011011001	00101111
12.55	11110011101	00101111
12.53	10011011101	00101111
12.34	10111011001	00111111

Table 3: Best chromosomes selected by the GA and the associated error percentage.

3.2 Temporal Monitoring using Dempster-Shafer Theory

3.2.1 Determination of the Hypotheses – Frame of Discernment

In order to exploit the textural measurements provided by the classifier for change/target detection and identification, a contextual database is built that will make the correspondence between the output of the classifier and the natural and/or man-made objects/structures we wish to monitor.

All texture measurement lead to a declaration characterizing the texture Each declaration is made of the four texture propositions WATER, WETLAND, VEGETATION, MAN-MADE OBJECT with an associated mass which represent the confidence level that the corresponding pixel actually belongs to this class. This frame of discernment must be completed by a set of alterations that may trigger a closer analysis. As an example, the declaration built from the texture measurement WATER will consist in the reunion of water (exclusive hypothesis), shore (possible alteration with WETLAND), flood (possible alteration with VEGETATION), ship (possible alteration with MAN-MADE OBJECT). In the same manner, the declaration built from the texture measurement WETLAND will consist in the reunion of wetland (exclusive hypothesis), shore (possible alteration with WATER), clear-cut (possible alteration with VEGETATION), vehicle (possible alteration with MAN-MADE OBJECT). The declaration built from the texture measurement VEGETATION will consist in the reunion of vegetation (exclusive hypothesis), flood (possible alteration with WATER), clear-cut (possible alteration with WETLAND), vehicle (possible alteration with MAN-MADE OBJECT). Finally, the declaration built from the texture measurement MAN-MADE OBJECT will consist in the reunion of building (exclusive hypothesis), ship (possible alteration with WATER), vehicle (possible alteration with WETLAND and VEGETATION).

The classifier is applied independently on each temporal scene that has been cautiously co-registered using an FFT-based method.

Table 4 shows the contextual database and how the confidence level of the textural measurement is spread among the various hypotheses compatible with the associated texture. To each texture declaration is attached an ignorance having a mass set to $(1 - \text{textural confidence level})$.

The first four columns of Table 4 represent the four generic hypotheses, their non-conflicting combination giving rise to the other five hypotheses. Then, the associated masses are normalized so that their sum is equal to 1.

The combination of conflicting and non-conflicting hypotheses in the textural declaration is used to interpret temporal changes. For example, the shore class will appear as water (submerged) in some images (high tide), and as wetland in others, and the result of the fusion process classify these changes over time as temporary submerged areas.

The same applies for the detection of ships resulting from the fusion of a man-made object detected on water. The difference is that the ship is there in one image and not in the other, as opposed to the sand which is always there, just partially hidden. However, we made the choice of considering ships as always present but sometimes hidden, since – for coastal surveillance purpose – it is desirable that ships appear at the end of the fusion process even if it is present on one image out of seven.

Those coefficients show that sand and ships classes can not be detected in a single image, but would appear by the fusion of two images giving different classifications.

Classes	Water	Wetland	Vegetation	Building	Shore	Flood	Ship	Clear-cut	Vehicle	Ignorance
WATER	0.44	0	0	0	0.18	0.18	0.18	0	0	0.02
WETLND	0	0.44	0	0	0.17	0	0	0.20	0.17	0.02
VEGET.	0	0	0.44	0	0	0.17	0	0.20	0.17	0.02
MMO	0	0	0	0.44	0	0	0.27	0	0.27	0.02

Table 4 – Contextual Database with coefficients used to spread the textural confidence level generated by the classifier.

Once the masses for all hypotheses are determined, declarations are fused using the Dempster-Shafer evidential theory [Dempster, 1968],[Shafer, 1976]. The resulting masses can be used as input for another fusion process with another image of the same area to improve even more the classification and monitor changes. Fusion using Dempster-Shafer theory is associative and can thus be used to combine declarations as they arrive without having to recompute the classification on the old images.

After each declaration fusion, a thematic map can be built by setting the value of the current pixel to the proposition associated to the highest mass.

4. Results

Following are examples of change monitoring and target detection applications on the RADARSAT-1 dataset acquired over the city of Stephenville (Newfoundland) and vicinity as provided by the Canadian Space Agency for the ADRO220 project.

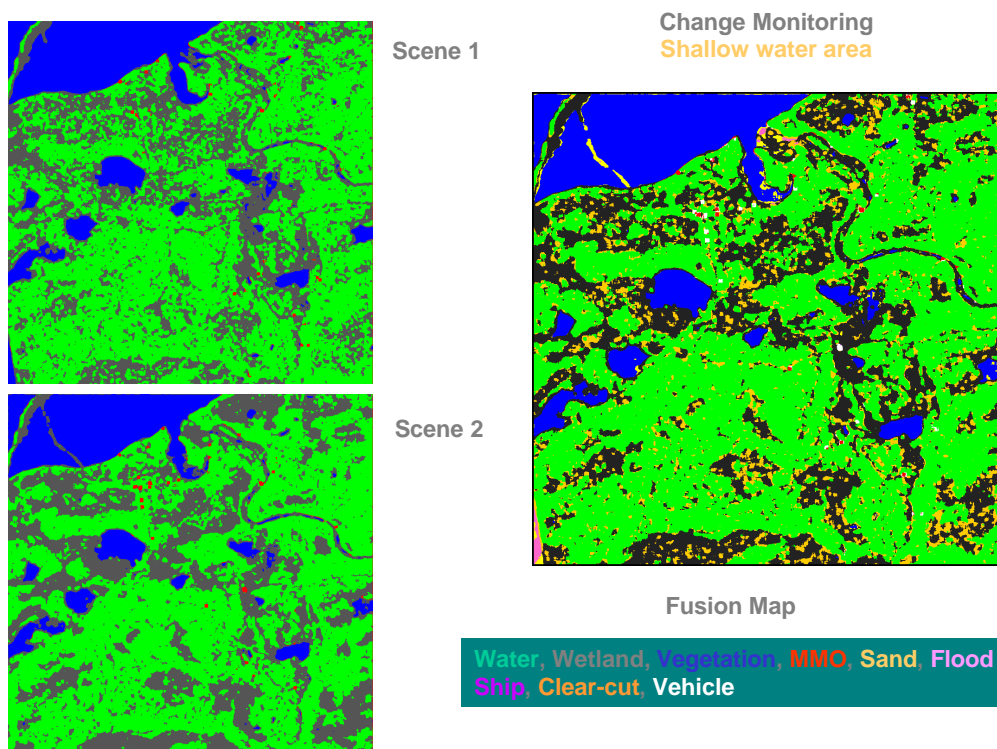


Figure 13 . Change Monitoring using Evidential Fusion

Figure 13 represents an area south of Saint-George Bay. The upper and lower left maps are the result of the classification that are fused in the map on the right.

These maps show that the classification of the arm between the peninsula and the land is covered by water in Scene1, and detected as wetland in Scene2. The fusion process combined the 2 images and classified the area as sand.

On the other hand, a bridge crossing the river is well detected in Scene 1 as man made object (MMO). On Scene2, due to different acquisition parameters, the bridge is not detected. The fusion process is designed in such a way that, on the fused image, the bridge that once was detected is still visible.

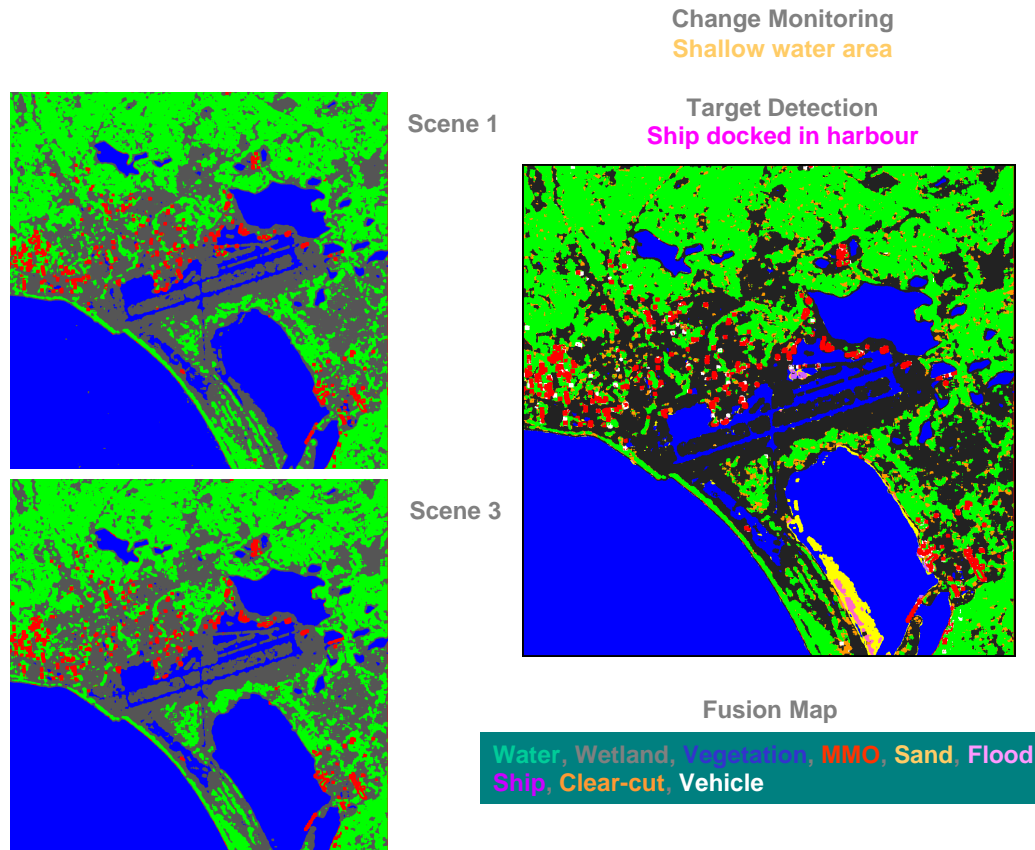


Figure 14 – Change Monitoring and Target Detection using Evidential Fusion.

Figure 14 shows the city of Stephenville, its airport and Port Harmon harbor. The upper and lower left maps are the result of the classification that is fused in the map on the right.

On the fused map, a ship is detected docked on a pier located at the east side of Port Harmon harbor. In the center of the image, the airport is detected as water, due to the fact that its texture is very similar to the texture of the water. Thus, the classifier detected a "ship" on the airport (as the airport is considered as water), which is probably a man made structure which has been temporarily placed on the airport. This misclassification could easily be solved by fusing the GIS themes (see Figures 4-12).

We can also notice the large zone detected as sand in the west of the bay area. This is confirmed by the water level (see Table 2), which is 0.607m in the Scene 1, June 14th 1998, and 0.982m in the Scene 3, May 25th 1998. There is a 20 cm difference between the 2 images, which explains the submerged area in the Scene 3 image.

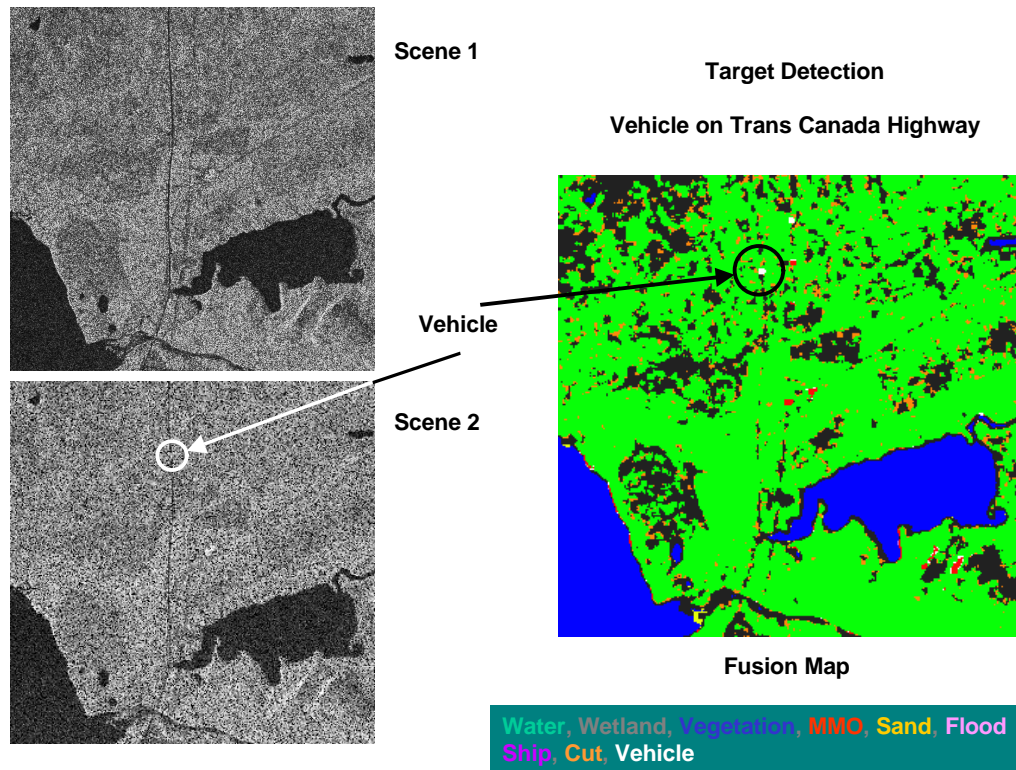


Figure 15 – Detection of a vehicle on the TransCanada Highway

Figure 15 shows a region on the eastern side of Stephenville, crossed by the Trans-Canada Highway. The main feature of these images is a Man Made Object (MMO) detected over an area classified as land that raised the hypothesis of a vehicle (or a big structure) that we detect on the middle of the road on the scene 2. The fusion process contributes to highlight the presence of this object.

5. Conclusion

We presented an application of coastal monitoring/target detection using evidential fusion. The results obtained so far are very promising, and can easily be adapted to other monitoring applications using multi-date imagery.

We are currently working on a more complex data fusion system using the evidential fusion of polarimetric features from SAR imagery and spectral features from hyperspectral data cubes.

6. References

- [Banerjee & al., 1999] Banerjee, A., Burling, P. and Alajaji, F., "Image Segmentation and Labeling using the Polya urn Model," *IEEE Transactions on Image Processing*, vol. 8, no. 9, pp. 1243-1253, 1999.
- [Besag, 1986] Besag, J., "On The Statistical Analysis of Dirty Pictures," *Journal of the Royal Statistical Society*, vol. 48, no. 3, p. 259-302, 1986.
- [Chellappa and Chatterjee, 1984] R. Chellappa, S. Chatterjee., "Classification of Textures Using Gaussian Markov Random Fields," *IEEE Transactions on Acoustics, Speech and Signal Processing*, v. ASSP 33.4, pp. 959 963, August 1984.
- [Dempster, 1968] Dempster A.P., "A Generalization of Bayesian Inference," *Journal of the Royal Statistical Society*, Vol. 30, serie B, 1968.
- [Geman & Geman, 1984] Geman, S. Geman, D., "Stochastic Relaxation, Gibbs Distribution and the Bayesian Restoration of Images," *IEEE Transaction on Pattern Analysis and Machine Intelligence*, vol. PAMI-6, no. 6, p. 452-472, 1984.
- [Kato, 1994] Kato, Z., "Modelisation markoviennes multiresolutions en vision par ordinateur. Application a la segmentation d'images SPOT," Ph. D. Thesis, Universite de Nice-Sophia Antipolis, 1994.
- [Kirkpatrick & al., 1983] Kirkpatrick, S. Gelatt, C., Vecchi, M., "Optimization by Simulated Annealing," *Science* 220, p. 671-680, 1983
- [Pony & al, 2000] Pony, O., Descombes, X. and Zerubia, J., "Classification d'images satellitaires hyperspectrales en zone rurale et periurbaine," *Research report no. 4008*, INRIA, France, 2000.
- [Shafer, 1976], Shafer G., A Mathematical Theory of Evidence, Princeton University Press, Princeton, 1976.
- [Solberg, 1997] Anne H. Schistad Solberg, Anil K. Jain, "Texture Analysis of SAR Images: A Comparative Study," *Technical report*, Norwegian computing center, 1997